Journal of Quantitative Spectroscopy & Radiative Transfer 185 (2016) 86–94

Contents lists available at ScienceDirect

Journal of Quantitative Spectroscopy & Radiative Transfer

journal homepage: www.elsevier.com/locate/jqsrt

Q-space analysis of light scattering by ice crystals

Yuli W. Heinson [a], Justin B. Maughan [a], Jiachen Ding [b], Amitabha Chakrabarti [a], Ping Yang [b], Christopher M. Sorensen [a,*]

[a] Department of Physics, Kansas State University, Manhattan, KS 66506, USA
[b] Department of Atmospheric Sciences, Texas A&M University, College Station, TX 77843, USA

ARTICLE INFO

Article history:
Received 28 June 2016
Received in revised form
29 August 2016
Accepted 29 August 2016

Keywords:
Light scattering
Ice crystal
Q-space analysis
Rayleigh normalization

ABSTRACT

Q-space analysis is applied to extensive simulations of the single-scattering properties of ice crystals with various habits/shapes over a range of sizes. The analysis uncovers features common to all the shapes: a forward scattering regime with intensity quantitatively related to the Rayleigh scattering by the particle and the internal coupling parameter, followed by a Guinier regime dependent upon the particle size, a complex power law regime with incipient two dimensional diffraction effects, and, in some cases, an enhanced backscattering regime. The effects of significant absorption on the scattering profile are also studied. The overall features found for the ice crystals are similar to features in scattering from same sized spheres.

1. Introduction

Significant theoretical and computational advances have been made for the problem of how non-spherical particles scatter light and relevant applications [1–15]. Various light-scattering computational methods have been successfully developed and applied to a wide range of shapes extending to large size parameters. These advances naturally lead to a challenge as how to physically interpret the result. It is desirable to have descriptive abilities that can compare the similarities and differences of the scattering by different types of particles. It is also desirable to be able to infer physical interpretation for the scattering mechanism.

This paper is concerned with the problem of how to interpret the scattering patterns that can be calculated for irregularly shaped particles. As detailed in Yang et al. [11], we use a combination of the discrete dipole approximation (DDA) method [16–18] and an improved geometric optics method (IGOM) [10] to calculate the scattering differential cross section of seven different types of ice crystals. The optical properties of ice particles are fundamental to the assessment of the radiative forcing of cirrus clouds that play an important role in the earth's climate system. To interpret the single-scattering properties, we use the method of Q-space analysis, which is described below. We find that Q-space analysis uncovers heretofore unseen characteristics that have both physical interpretation as well as descriptive ability. In particular, we find many common features between the ice crystals and with spherical particles as well as features that can distinguish particle shapes.

2. Q-space analysis applied to spheres

Q-space analysis [19–21] involves plotting the scattered intensity, as embodied in the differential scattering cross section and proportional to the phase function, versus the dimensionless variable qR, where q is the magnitude of the scattering wave vector, $q = (4\pi/\lambda)\sin(\theta/2)$ with λ is the wavelength of light and θ the scattering angle, and where R is the particle effective radius. The plot is double logarithmic. Q-space analysis reveals functionalities of the

* Corresponding author.
E-mail address: sor@phys.ksu.edu (C.M. Sorensen).

http://dx.doi.org/10.1016/j.jqsrt.2016.08.021
0022-4073/

scattering with q that are not apparent with conventional plotting with the scattering angle θ, and, indeed, its application to ice crystal scattering is the primary motive of this paper. Often in Q-space analysis, the differential cross section is normalized by the Rayleigh differential cross section of the particle, which for a sphere is given by [22–24]

$$dC_{sca,Ray,sph}/d\Omega = k^4R^6F(m), \tag{1}$$

where $k = 2\pi/\lambda$ and

$$F(m) = \left|\frac{m^2-1}{m^2+2}\right|^2 \tag{2}$$

is the square of the Lorentz–Lorenz factor for a refractive index of $m = n + i\kappa$. Plots of the Rayleigh normalized scattering in Q-space for different spheres closely align when their internal coupling parameters are equal. The internal coupling parameter ρ' for a sphere is given by [25]

$$\rho' = 2kR\sqrt{F(m)} = 2kR\left|\frac{m^2-1}{m^2+2}\right| \tag{3}$$

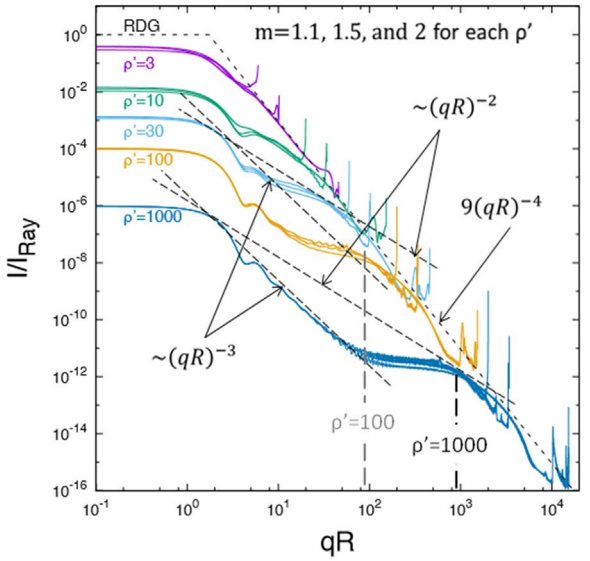

Fig. 1. Q-space analysis of spheres for the RDG limit and $\rho' = 3,\ 10,\ 30,\ 100$, and 1000. The scattering curves with the same ρ' fall on top of each other (despite widely ranging R and m).

Fig. 1 shows Q-space analysis applied to scattering by spheres (Mie scattering). Shown are plots for the Rayleigh Debye Gans (RDG) limit, which occurs when $\rho' \to 0$, and $\rho' = 3,\ 10,\ 30,\ 100$, and 1000. The Rayleigh normalized differential cross section is represented by a normalized intensity, I/I_{Ray}. A small size distribution (20% log-normal size distribution) has been applied to eliminate the interference ripples.

The scattering curves in Fig. 1 with the same ρ' fall on top of each other (despite widely ranging R and $m = 1.1, 1.5$, and 2 for each ρ') [26]. It is important to know that the RDG limit is simply the square of the Fourier transform of the spherical shape, and thus is the three-dimensional (3d) Fraunhofer diffraction by that shape. The envelope of the RDG scattering is $9(qR)^{-4}$ and shown in Fig. 1. From this diffraction limit the rest of the scattering evolves with increasing ρ'. For all ρ' a forward scattering lobe of constant intensity appears when $qR < 1$. With increasing qR, the scattering begins to decrease in the Guinier regime near $qR \simeq 1$. For $\rho' < 1$, the RDG limit, a $(qR)^{-4}$ functionality follows the Guinier. When ρ' gets large, $\rho' \gtrsim 30$, a $(qR)^{-3}$ functionality (2d Fraunhofer diffraction, see below) starts to appear after the Guinier regime. The $(qR)^{-3}$ regime is followed by a "hump" regime which then crosses over to approximately the same $(qR)^{-4}$ functionality of the RDG limit when $qR \gtrsim \rho'$. Connecting the Guinier regime and the hump regime with an equal tangent line gives a $(qR)^{-2}$ functionality which dominates, albeit briefly and imperfectly, when $\rho' < 10$. Finally, at largest qR near $2kR$, enhanced backscattering occurs. We call the region between the Guinier regime and the backscattering the power law regime.

Fig. 2 shows the Rayleigh normalized forward scattering, $I(0)/I_{Ray}$, as a function of ρ' for spheres [25]. Fig. 2 demonstrates that when $\rho' < 1$, $I(0) = I_{Ray}$, but when $\rho' > 10$, $I(0) = I_{Ray}/\rho'^2$. This is described in Eqs. (4).

$$I(0) = I_{Ray} \text{ when } \rho' \lesssim 1 \tag{4a}$$

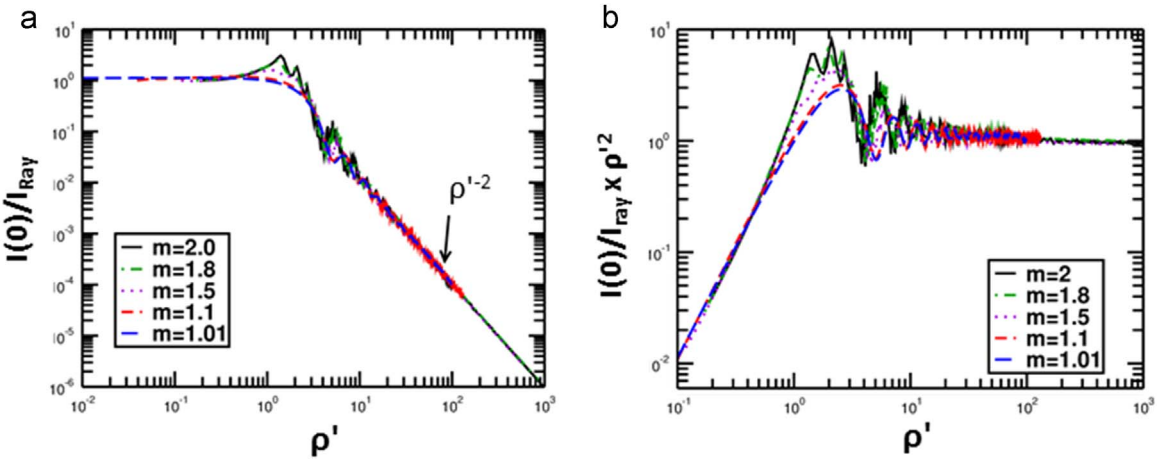

Fig. 2. (a) Rayleigh normalized forward scattering, $I(0)/I_{Ray}$, versus ρ'; **(b)** Rayleigh normalized forward scattering multiplied by ρ'^2 versus ρ' [25].

$$I(0) = I_{Ray}/\rho'^2 \text{ when } \rho' \gtrsim 10 \quad (4b)$$

Between these limits, a ripple structure ensues.

3. Q-space analysis applied to ice crystals

The same Q-space analysis has been applied to ice crystal habits/shapes considered in a database of the single-scattering properties reported by Yang et al. [11]. Nine shapes were studied: droxtal, plate, 5-plate aggregate, 10-plate aggregate, solid column, 8-column aggregate, hollow column, solid column rosette, and hollow column rosette. Three degrees of surface roughness, namely, $\sigma = 0.0$ (smooth), $\sigma = 0.03$ (moderately rough), and $\sigma = 0.5$ (severely rough), for each ice crystal habit. The physical meaning of the roughness parameter σ is described in detail in Yang and Liou [27].

Here Q-space analysis will be applied to the Rayleigh normalized scattered intensities of these ice crystals. Doing this requires generalization of the formulae for Rayleigh scattering, Eqs. (1) and (2), and the internal coupling parameter, Eq. (3), to non-spherical shapes. We have recently developed such a formulation [28], which we now briefly describe.

In general the Rayleigh differential cross section goes as [22,28]

$$dC_{sca,Ray}/d\Omega = k^4 V^2 |\alpha(m)|^2 \quad (5)$$

where V is the volume of the particle and $\alpha(m)$ the average volume polarizability [22], which is dependent on the shape and the complex index of refraction m. To calculate the shape and index dependent $\alpha(m)$, ADDA [17] a well-known and widely used software for calculating the scattering by arbitrary shapes is used. The differential cross section in the forward direction i.e. $(\theta = 0)$ divided by k^4 is plotted vs V^2 the slope of which determines $|\alpha(m)|^2$ and thus $\alpha(m)$. Once $\alpha(m)$ is known it can be used to calculate the Rayleigh scattering for any combination of λ and volume within the Rayleigh limit for a given shape and index m. Furthermore, this leads to a general definition of the internal coupling parameter of which Eq. (3) is a specific case for spheres. The internal coupling parameter for any arbitrary shape is defined as [28]

$$\rho' = 2\pi k \frac{V}{A} \alpha(m) \quad (6)$$

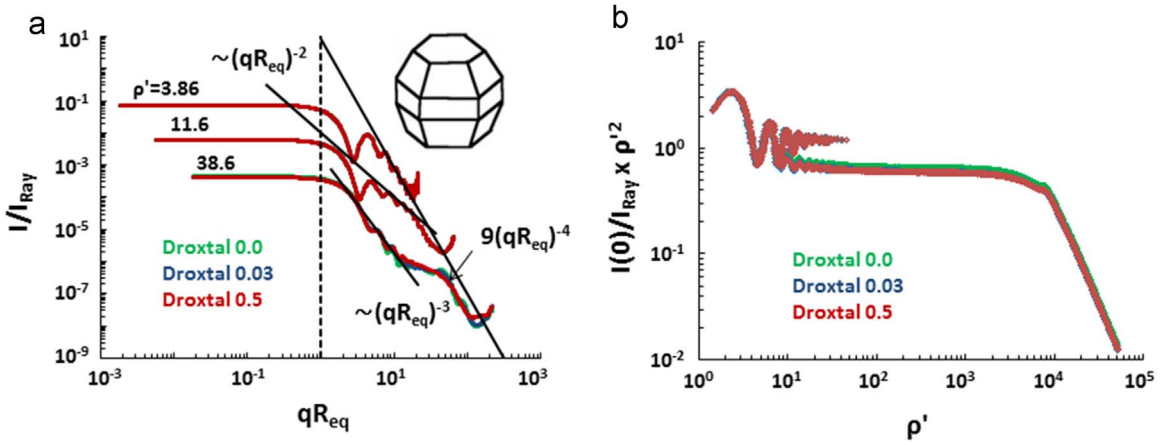

Fig. 3. **(a)** Q-space analysis of droxtal for $\rho' = 3.86$, 11.6, and 38.6 with three degrees of surface Roughness. **(b)** Test of the forward scattering functionality with ρ' as described by Eqs. (4).

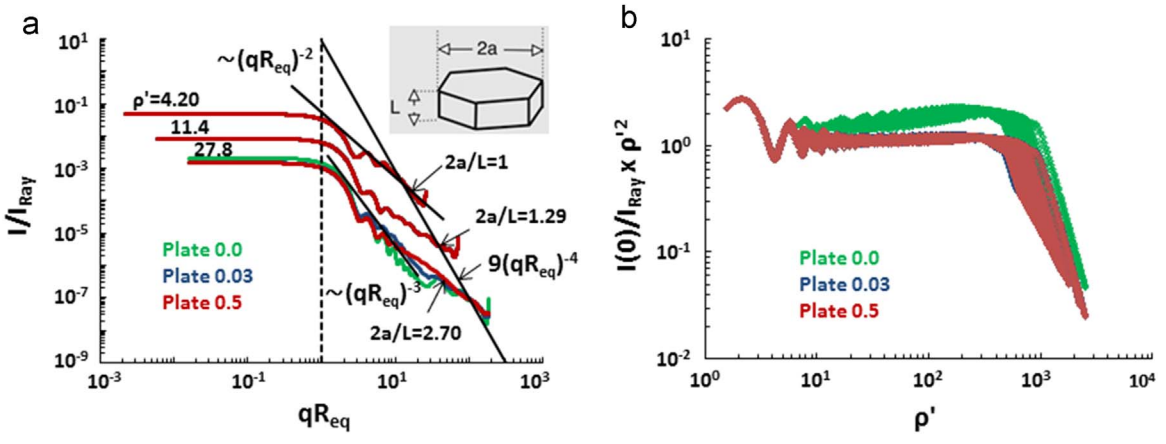

Fig. 4. **(a)** Q-space analysis of plate for $\rho' = 4.20$, 11.4, and 27.8 with three degrees of surface Roughness. (b) Test of the forward scattering functionality with ρ' as described by Eqs. (4).

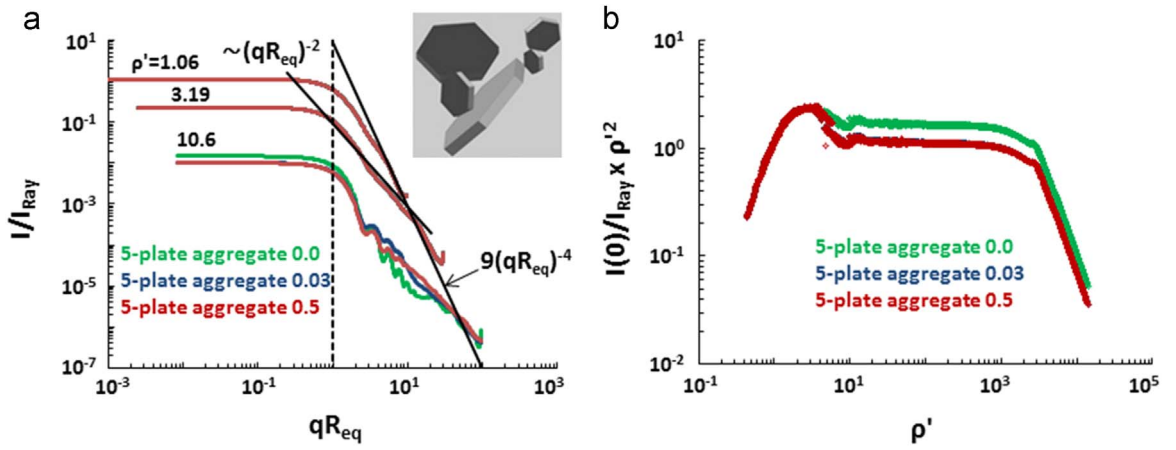

Fig. 5. **(a)** Q-space analysis of 5-plate aggregate for $\rho' = 1.06$, 3.19, and 10.6 with three degrees of surface Roughness. **(b)** Test of the forward scattering functionality with ρ' as described by Eqs. (4).

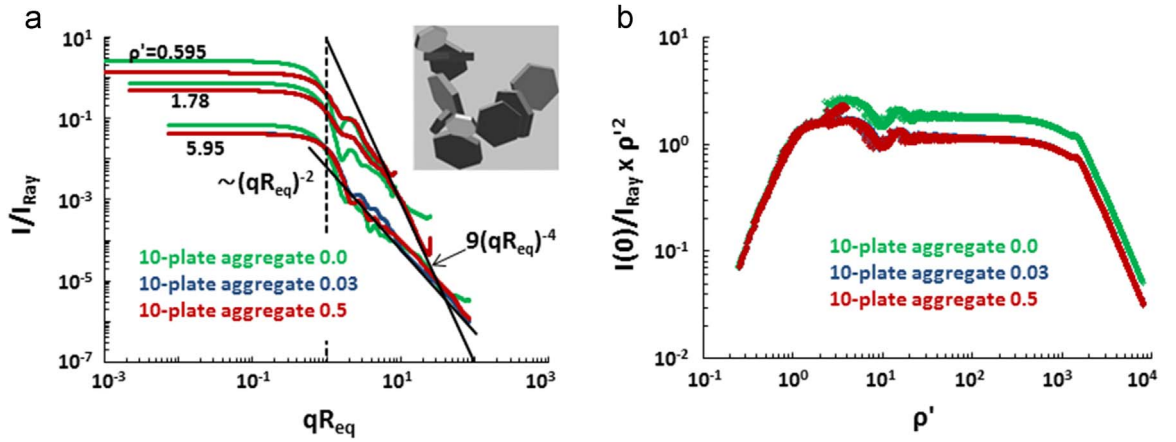

Fig. 6. **(a)** Q-space analysis of 10-plate aggregate for $\rho' = 0.595$, 1.78, and 5.95 with three degrees of surface Roughness. **(b)** Test of the forward scattering functionality with ρ' as described by Eqs. (4).

where A is the projected area of the scatterer in the direction of the incident light. This formulation is applied to the ice crystal scattering below.

Figs. 3(a)–11(a) present the Q-space analysis of the angular scattering functionality, proportional to the phase function, for the ice crystals. The optical wavelength was $\lambda = 0.53\mu m$, the maximum dimensions of the various shapes were $D = 2$, 6 and 20 μm and the refractive index was $m = 1.31$. We plot I/I_{Ray} vs. qR_{eq}, where R_{eq} is volume equivalent radius. Corresponding ρ's for maximum dimensions $D = 2$,6,20 μm are labeled next to the scattering curves.

In all cases the scattering evolves with increasing ρ' in a manner similar to spheres and has patterns similar to those of spheres: a constant intensity forward scattering lobe is followed by a Guinier regime, a complex power law regime, and sometimes an enhanced backscattering regime. Enhanced backscattering does not occur for aggregate-like ice crystals and hollow columns. Except for 10-plate aggregate, the scattering curves fall on top of each other for different degrees of surface roughness when ρ' is small ($\rho' \lesssim 10$). When ρ' gets bigger, the scattering curves start to show slight differences for different degrees of surface roughness. Also, roughness tends to smooth the scattering curves.

We now study these regimes separately and in detail.

3.1. The Guinier regime

The Guinier regime for most of the ice crystals is well marked by $qR_{eq} \simeq 1$. This is the same as for spheres although spheres show some deviations with increasing refractivity [29]. We will not explore that detail here and remain content with the semi-quantitative equivalence of spheres and ice crystals in the Guinier regime. Larger deviation exists, however, with the 5-plate aggregate and 10-plate aggregate shapes. We propose that this is due to their open, aggregate morphology which would have a radius of gyration R_g much bigger than the volume equivalent radius R_{eq}. The Guinier equation for any shape is given by [30]

$$I(q) = I(0)\left(1 - (qR_g)^2/3\right) \tag{7}$$

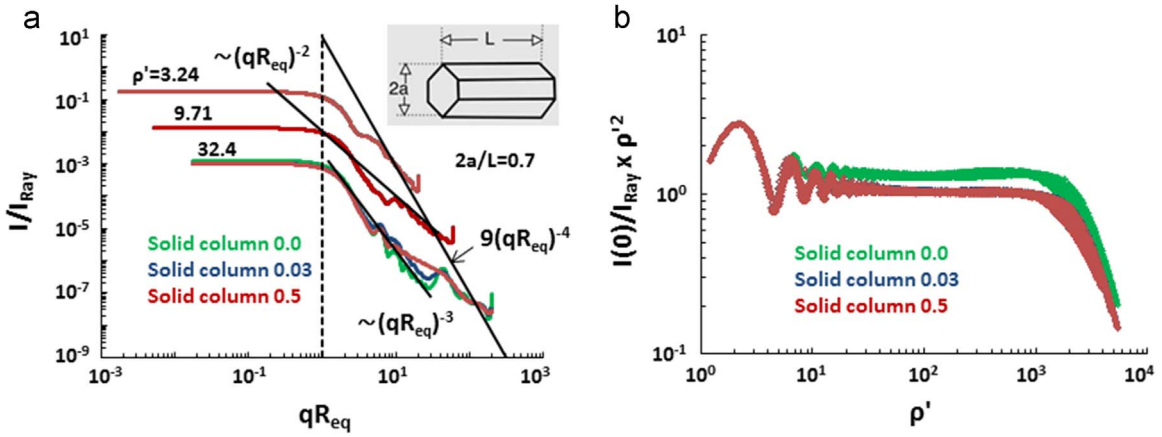

Fig. 7. (a) Q-space analysis of solid column for $\rho' = 3.24$, 9.71, and 32.4 with three degrees of surface Roughness. **(b)** Test of the forward scattering functionality with ρ' as described by Eqs. (4).

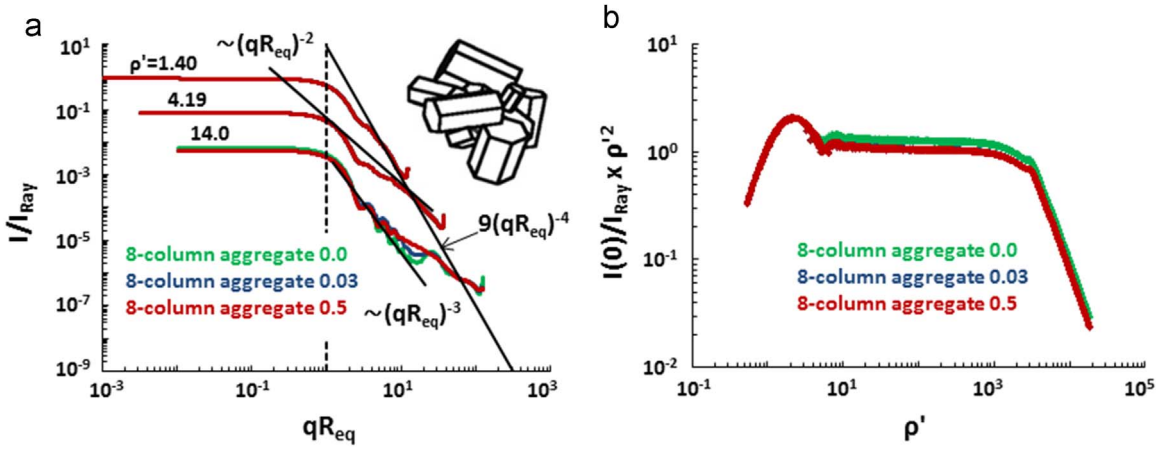

Fig. 8. (a) Q-space analysis of 8-column aggregate for $\rho' = 1.40$, 4.19, and 14.0 with three degrees of surface roughness. (b) Test of the forward scattering functionality with ρ' as described by Eqs. (4).

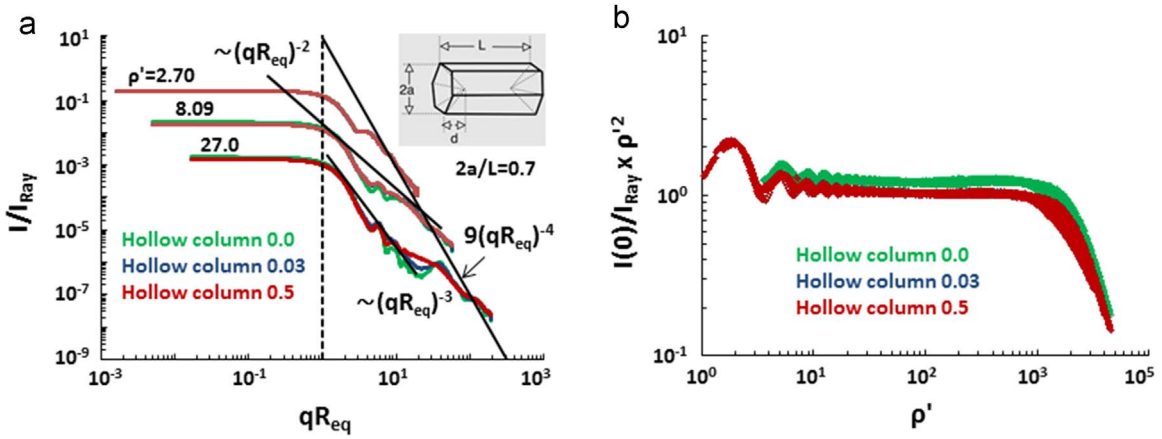

Fig. 9. (a) Q-space analysis of hollow column for $\rho' = 2.70$, 8.09, and 27.0 with three degrees of surface roughness. **(b)** Test of the forward scattering functionality with ρ' as described by Eqs. (4).

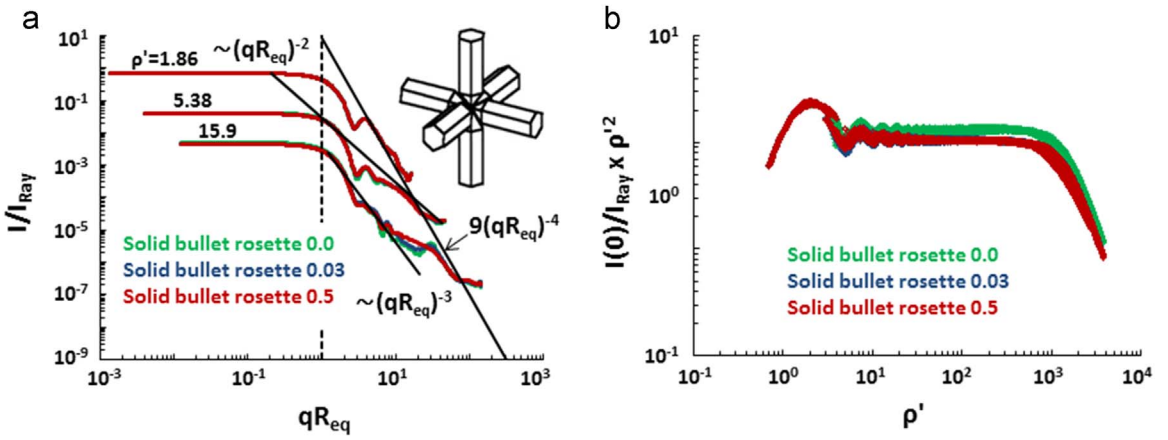

Fig. 10. **(a)** Q-space analysis solid bullet rosette for $\rho' = 1.86$, 5.38, and 15.9 with three degrees of surface roughness. **(b)** Test of the forward scattering functionality with ρ' as described by Eqs. (4).

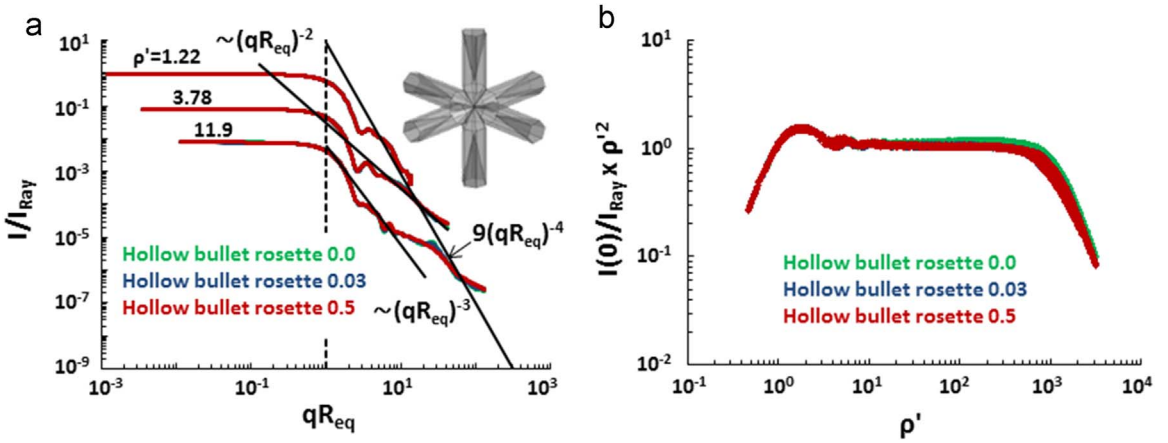

Fig. 11. **(a)** Q-space analysis of hollow bullet rosette for $\rho' = 1.22$, 3.78, and 11.9 with three degrees of surface roughness. **(b)** Test of the forward scattering functionality with ρ' as described by Eqs. (4).

For a sphere, the geometric radius $R = R_{eq} = \sqrt{5/3}R_g$. However, for an aggregate R_g could be much bigger than R_{eq}. Thus plotting $I(qR_{eq})$ versus qR_{eq} for an aggregate will cause the Guinier regime to appear at qR_{eq} values smaller than one, which is what is observed. Thus we conclude that the Guinier equation applies for these ice aggregates when R_g is used.

3.2. The power law regime

Most of the ice crystals show a rough -2 power law when $\rho' \simeq 5$–10 which gives over, with increasing ρ', to the -2 power law becoming an equal tangent line between the Guinier regime and the hump near $qR \simeq \rho'$. At the largest ρ' values, typically in the range 20–30, a brief -3 power law appears extending from the Guinier regime under this equal tangent -2 power law with increasing qR_{eq}. After that, follows the hump near $qR \simeq \rho'$. All this behavior is quite similar to that seen for spheres and demonstrated in Fig. 1.

Eventually, when $qR_{eq} \gtrsim \rho'$, the scattering touches on, and in some cases follows, the $9(qR)^{-4}$ functionality of the RDG formula for spheres. This is similar to sphere behavior in that the scattering obtains intensities approximately equal to that given by RDG. However, the ice crystal scattering typically crosses the RDG line, whereas the sphere scattering approaches the line and then curves away with a stronger decline.

The -3 power law that occurs for spheres when $\rho' \gtrsim 30$ is due to the onset of two-dimensional (2d) Fraunhofer diffraction (the Airy pattern) from the projected geometric circular cross section of the sphere. One can show that diffraction from any d-dimensional object will contain interference ripples with a $q^{-(d+1)}$ envelope [31]. Thus we conclude that the onset of a -3 power law regime, albeit brief, in the non-aggregate ice crystal scattering is due to the projection of their 3d shapes into two dimensions.

We note that the hump near $qR \simeq \rho'$ for many of the ice crystals shows strong structure for the non-rough (smooth) $\sigma = 0.0$ situations. With increasing roughness, these quick variations relax to the hump.

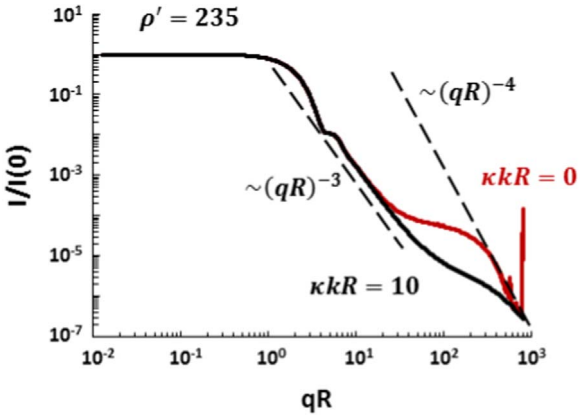

Fig. 12. Comparison between the scattered light from spheres with $\rho' = 235$ and $\kappa kR = 0$ (without absorption) and $\kappa kR = 10$ (with absorption). Spheres with absorption lost the hump and glory leaving the $(qR)^{-3}$.

The ice crystal aggregates, 5-plate aggregate and 10-plate aggregate, do not follow the same sphere like behavior. For both, but more so for the 10-plate aggregate, a more uniform power law regime is seen, consistent with the known scattering behavior for fractal aggregates which display one, uniform power law in their scattering [32]. Although these aggregates have only five and ten primary particles and hence are not fully developed aggregates, these results hint at the concept that aggregates are a fundamentally different type irregular shape than the ice crystals. We have proposed this same concept in our studies of scattering from dusts [33].

3.3. The backscattering regime

A definite pattern to the backscattering for the ice crystals is difficult to discern. Backscattering, if it occurs, starts near (to within a factor of 3) the RDG $9(qR_{eq})^{-4}$envelope. In many cases it is less pronounced at the largest value of ρ'. Beyond these simple observations, any patterns that might exist in backscattering remain hidden.

3.4. The forward scattering regime

Figs. 3(b)–11(b) study the Rayleigh normalized forward scattering $I(0)/I_{Ray}$ for the ice crystals. Plotted is $I(0)/I_{Ray} \times \rho'^2$ vs. ρ' for ice crystals without absorption. The same functionality was plotted for spheres in Fig. 2b. The Rayleigh normalization for the ice crystal shapes is our generalized scheme describe in Eqs. (5) and (6).

Figs. 3(b)–11(b) verify Eq. (4b) when $\rho' \gtrsim 10$ for ice crystals with roughness $\sigma = 0.03$ and 0.5; that is, the forward scattering behavior with ρ' for the ice crystals is identical to that of spheres, Eq. (4b). However, while the curves for $\sigma = 0.03$ and 0.5 are overlapping with each other, the data $\sigma = 0.0$ for smooth crystals deviate by factors as large as 2. When $\rho' > 10^3$, the data begin a drastic deviation from Eq. (4b). This is because the IGOM, which was used to calculate the scattering data for large size, is less applicable in terms of accuracy in this size regime.

For the ice crystals where the data exist for $\rho' < 1$, Eq. (4a) is also verified. The transition region, $1 \lesssim \rho \lesssim 10$, for some of the crystals has an oscillatory behavior similar to that for spheres; about the same period of $\Delta\rho' \simeq 3.8$ but smaller in amplitude. However, aggregates (specifically, 5-plate aggregate, 8-plate aggregate, and 10-column aggregate) have a single maximum in this region. Moreover, a physical interpretation of the results for droxtals requires a further investigation.

4. Consequences of absorption

A non-zero imaginary part of the refractive index, κ, will cause absorption. However, we have shown for spheres that significant absorption, such that the scattering phase function changes, is governed by the parameter κkR [34]. When $\kappa kR < 0.3$, absorption is relatively insignificant; when $\kappa kR > 3$, absorption is significant. Physically, κkR is the ratio of the particle radius to the absorption skin depth.

Fig. 12 shows the scattering by a narrow distribution of large, refractive spheres with $\rho' = 235$ and $\kappa kR = 0$ (without absorption) and $\kappa kR = 10$ (with significant absorption). Compared to the spheres without absorption, the scattering of spheres with absorption lost most of the hump and all of the glory leaving the $(qR)^{-3}$ power law [34].

Figs. 13 and 14 study the effects of absorption on ice crystals. Fig. 13 shows the scattering by Droxtal with $\rho' = 830$ and $\kappa kR_{eq} = 0$ and $\kappa kR_{eq} = 85$ for three degrees of surface roughness; the scattering of the volume equivalent spheres are included for comparison. Fig. 14 shows the scattering by Solid column with $\rho' = 140$ and $\kappa kR_{eq} = 0$ and $\kappa kR_{eq} = 20$ for three degrees of surface Roughness; the scattering of the volume equivalent spheres are included for comparison. In order to compare the scattered light from ice crystals with and without absorption, large crystals were chosen so that κkR was large.

Similar as spheres, for both the Droxtal and the Solid column with absorption, the hump and glory disappear leaving predominately the $\left(qR_{eq}\right)^{-3}$ power law. Also remaining is the tendency to approach the spherical particle RDG $(qR)^{-4}$ functionality. For the ice crystals without absorption, the scattering of the ice crystal with the roughest surface ($\sigma = 0.5$) is the closest to the scattering due to the volume equivalent spheres, compare to the other two degrees of surface roughness, $\sigma = 0.0$ and 0.03. For the ice crystals with absorption the scattering curves fall on top of each other regardless the roughness. Notice that the Solid column with absorption shows two Guinier regimes which appears to be strange. However, the corresponding shape profile claims that $L/2a \approx 10$ which matches the separation between the two Guinier regimes. Furthermore, the corresponding qR_{eq} values at the two Guinier regimes match $(L/R_{eq})^{-1}$ and $(2a/R_{eq})^{-1}$.

5. Conclusions

There are many common features between scattering by spheres and a wide variety of ice crystals. These

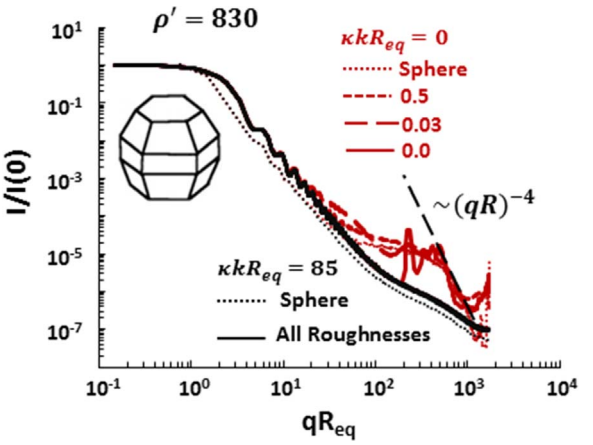

Fig. 13. Comparisons between the light scattered from Droxtal with and without absorption and volume equivalent spheres. Both the Droxtal and the sphere with absorption lose the hump and the glory.

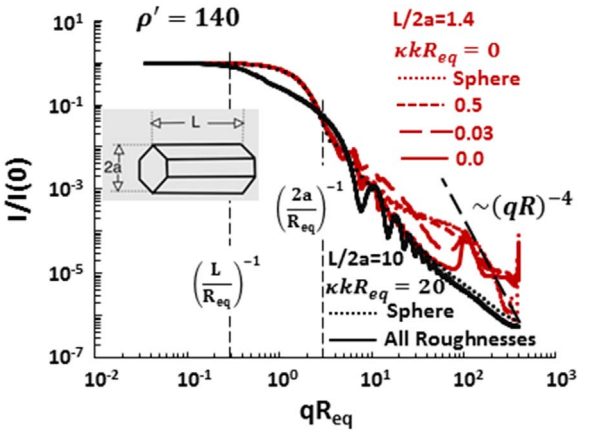

Fig. 14. Comparisons between the light scattered from two Solid column structures with different aspect ratios with and without absorption and volume equivalent spheres. Both the Solid column and the sphere with absorption lose the hump and the glory. Note also the two Guinier regimes for the Solid column with $\kappa kR_{eq} = 20$ match $qR_{eq} = (L/R_{eq})^{-1}$ and $qR_{eq} = (2a/R_{eq})^{-1}$.

features evolve in a quasi-universal manner with the internal coupling parameter ρ'. These features are:

1. A forward scattering lobe of constant intensity when $qR_{eq} < 1$. The intensity in this regime is the Rayleigh scattered intensity when the internal coupling parameter is $\rho' < 1$ and the Rayleigh scattering divided by ρ'^2 when $\rho' > 10$, as described in Eqs. (4).
2. A Guinier regime near $qR_{eq} \simeq 1$. Because this is an obvious bend in the scattering curve, a semi-quantitative measurement of the particle size can be determined from the inverse of the q-value where the bend occurs [30,35].
3. A complex power law regime when $1 \lesssim qR_{eq} < 2kR$. For non-aggregate crystals in this regime a $(qR_{eq})^{-3}$ functionality starts to occur with increasing ρ' which can be ascribed to 2d diffraction from the projected crystal shape. A hump structure appears centered near ρ'. At larger qR_{eq}, there is a tendency to approach the RDG $9(qR_{eq})^{-4}$ functionality of the RDG spherical particle limit. Significant absorption, as quantified by κkR, removes the hump. Aggregate ice crystals tend to have a smoother power law regime similar to fractal aggregates.
4. In many cases the ice crystals have enhanced backscattering near $qR_{eq} \simeq 2kR_{eq}$, which is equivalent to a scattering angle of $\theta = 180^{\circ}$. However, no systematic trends were discerned.

Surface roughness plays a minor role in these features except in the hump region where smooth surfaces give a wavy structure to the hump.

Finally, we note that these features would be difficult if not impossible to see without Q-space analysis.

Acknowledgements

This work was supported by the National Science Foundation (NSF) under Grant no. AGM 1261651 and the Army Research Laboratory under Grant no. W911NF-14-1-0352 (C.M.S.), and partly by NSF Grant no. AGS-1338440 (P.Y.).

References

[1] Dubovik O, Sinyuk A, Lapyonok T, Holben BN, Mishchenko M, Yang P, et al. Application of spheroid models to account for aerosol particle nonsphericity in remote sensing of desert dust. J Geophys Res-Atmos 2006;111:D11208. http://dx.doi.org/10.1029/2005JD006619.

[2] Kalashnikova OV, Sokolik IN. Modeling the radiative properties of nonspherical soil-derived mineral aerosols. J Quant Spectrosc Radiat Transf 2004;87:137–66. http://dx.doi.org/10.1016/j.jqsrt.2003.12.026.

[3] Muinonen K. Introducing the Gaussian shape hypothesis for asteroids and comets. Astron Astrophys 1998;332:1087–98.

[4] Maughan JB, Sorensen CM, Chakrabarti A. Q-space analysis of light scattering by Gaussian Random Spheres. J Quant Spectrosc Radiat Transf 2016;174:14–21. http://dx.doi.org/10.1016/j.jqsrt.2015.12.002.

[5] Muinonen K, Zubko E, Tyynela J, Shkuratov YG, Videen G. Light scattering by Gaussian random particles with discrete-dipole approximation. J Quant Spectrosc Radiat Transf 2007;106:360–77. http://dx.doi.org/10.1016/j.jqsrt.2007.01.049.

[6] Munoz O, Volten H, Hovenier JW, Nousiainen T, Muinonen K, Guirado D, et al. Scattering matrix of large Saharan dust particles: experiments and computations. J Geophys Res-Atmos 2007;112:D13215. http://dx.doi.org/10.1029/2006JD008074.

[7] Nousiainen T, Munoz O, Lindqvist H, Mauno P, Videen G. Light scattering by large Saharan dust particles: comparison of modeling and experimental data for two samples. J Quant Spectrosc Radiat Transf 2011;112:420–33. http://dx.doi.org/10.1016/j.jqsrt.2010.09.003.

[8] Sorensen CM, Zubko E, Heinson WR, Chakrabarti A. Q-space analysis of scattering by small irregular particles. J Quant Spectrosc Radiat Transf 2014;133:99–105. http://dx.doi.org/10.1016/j.jqsrt.2013.07.020.

[9] Veihelmann B, Nousiainen T, Kahnert M, van der Zande WJ. Light scattering by small feldspar particles simulated using the Gaussian random sphere geometry. J Quant Spectrosc Radiat Transf 2006;100:393–405. http://dx.doi.org/10.1016/j.jqsrt.2005.11.053.

[10] Yang P, Liou KN. Geometric-optics-integral-equation method for light scattering by nonspherical ice crystals. Appl Opt 1996;35:6568–84. http://dx.doi.org/10.1364/AO.35.006568.

[11] Yang P, Bi L, Baum BA, Liou K-N, Kattawar GW, Mishchenko MI, et al. Spectrally consistent scattering, absorption, and polarization properties of atmospheric ice crystals at wavelengths from 0.2 to 100 mu m. J Atmos Sci 2013;70:330–47. http://dx.doi.org/10.1175/JAS-D-12-039.1.

[12] Yang P, Liou K-N, Bi L, Liu C, Yi B, Baum BA. On the radiative properties of ice clouds: light scattering, remote sensing, and radiation parameterization. Adv Atmos Sci 2015;32:32–63. http://dx.doi.org/10.1007/s00376-014-0011-z.

[13] Zubko E, Shkuratov Y, Kiselev NN, Videen G. DDA simulations of light scattering by small irregular particles with various

structure. J Quant Spectrosc Radiat Transf 2006;101: 416–34. http://dx.doi.org/10.1016/j.jqsrt.2006.02.055.
[14] Zubko E, Shkuratov Y, Mishchenko M, Videen G. Light scattering in a finite multi-particle system. J Quant Spectrosc Radiat Transf 2008;109:2195–206. http://dx.doi.org/10.1016/j.jqsrt.2008.03.007.
[15] Zubko E, Kimura H, Shkuratov Y, Muinonen K, Yamamoto T, Okamoto H, et al. Effect of absorption on light scattering by agglomerated debris particles. J Quant Spectrosc Radiat Transf 2009;110: 1741–9. http://dx.doi.org/10.1016/j.jqsrt.2008.12.006.
[16] Purcell E, Pennypac cr. Scattering and absorption of light by nonspherical dielectric grains. Astrophys J 1973;186: 705–14. http://dx.doi.org/10.1086/152538.
[17] Yurkin MA, Hoekstra AG. The discrete-dipole-approximation code ADDA: capabilities and known limitations. J Quant Spectrosc Radiat Transf 2011;112:2234–47. http://dx.doi.org/10.1016/j.jqsrt.2011.01.031.
[18] Yurkin MA, Maltsev VP, Hoekstra AG. The discrete dipole approximation for simulation of light scattering by particles much larger than the wavelength. J Quant Spectrosc Radiat Transf 2007;106: 546–57. http://dx.doi.org/10.1016/j.jqsrt.2007.01.033.
[19] Sorensen CM, Fischbach DJ. Patterns in Mie scattering. Opt Commun 2000;173:145–53. http://dx.doi.org/10.1016/S0030-4018(99)00624-0.
[20] Berg MJ, Sorensen CM, Chakrabarti A. Patterns in Mie scattering: evolution when normalized by the Rayleigh cross section. Appl Opt 2005;44:7487–93. http://dx.doi.org/10.1364/AO.44.007487.
[21] Sorensen CM. Q-space analysis of scattering by particles: a review. J Quant Spectrosc Radiat Transf 2013;131: 3–12. http://dx.doi.org/10.1016/j.jqsrt.2012.12.029.
[22] Hulst HC van de. Light scattering by small particles. New York: Wiley; 1957.
[23] Kerker M. In: The scattering of light and other electromagnetic radiation. New York: Academic Press; 1969.
[24] Bohren CF, Huffman DR. In: Absorption and scattering of light by small particles. New York: Wiley; 1983.
[25] Heinson WR, Chakrabarti A, Sorensen CM. A new parameter to describe light scattering by an arbitrary sphere. Opt Commun 2015;356:612–5. http://dx.doi.org/10.1016/j.optcom.2015.08.067.
[26] Heinson WR, Chakrabarti A, Sorensen CM. Crossover from spherical particle Mie scattering to circular aperture diffraction. J Opt Soc Am -Opt Image Sci Vis 2014;31: 2362–4. http://dx.doi.org/10.1364/JOSAA.31.002362.
[27] Yang P, Liou KN. Single-scattering properties of complex ice crystals in terrestrial atmosphere. Contrib Atmos Phys 1998;71:223–48.
[28] Maughan JB, Sorensen CM, Chakrabarti A. Rayleigh Scattering and the Internal Coupling Parameter for Arbitrary Shapes. Manuscript in preparation.
[29] Sorensen CM, Shi D. Guinier analysis for homogeneous dielectric spheres of arbitrary size. Opt Commun 2000;178: 31–6. http://dx.doi.org/10.1016/S0030-4018(00)00601-5.
[30] Guinier A, Fournet G. In: Small-angle scattering of X-rays.Wiley; 1955.
[31] Oh C, Sorensen CM. Scaling approach for the structure factor of a generalized system of scatterers. J Nanopart Res 1999;1: 369–77. http://dx.doi.org/10.1023/A:1010033111039.
[32] Sorensen CM. Light scattering by fractal aggregates: a review. Aerosol Sci Technol 2001;35:648–87. http://dx.doi.org/10.1080/02786820117868.
[33] Heinson YW, Maughan JB, Heinson WR, Chakrabarti A, Sorensen CM. Light scattering Q-space analysis of irregularly shaped particles. J Geophys Res-Atmos 2016;121:682–91. http://dx.doi.org/10.1002/2015JD024171.
[34] Wang G, Chakrabarti A, Sorensen CM. Effect of the imaginary part of the refractive index on light scattering by spheres. J Opt Soc Am -Opt Image Sci Vis 2015;32:1231–5. http://dx.doi.org/10.1364/JOSAA.32.001231.
[35] Sorensen CM, Shi D. Guinier analysis for homogeneous dielectric spheres of arbitrary size. Opt Commun 2000;178:31–6.